Production of pi(0) and eta mesons in Cu plus Au collisions at root S-NN=200 GeV

PHENIX Collaboration

2018-11-19

PHENIX Collaboration , Aidala , C , Kim , D J , Krizek , F , Novitzky , N & Rak , J 2018 , ' Production of pi(0) and eta mesons in Cu plus Au collisions at root S-NN=200 GeV ' , Physical Review C , vol. 98 , no. 5 , 054903 . https://doi.org/10.1103/PhysRevC.98.054903

http://hdl.handle.net/10138/272985
https://doi.org/10.1103/PhysRevC.98.054903

Production of π^0 and η mesons in Cu + Au collisions at $\sqrt{s_{NN}} = 200$ GeV

C. Aidala,[39,44] N. N. Ajitanand,[62,*] Y. Akiba,[57,58,†] R. Akimoto,[12] J. Alexander,[62] M. Alfred,[24] K. Aoki,[32,57] N. Apadula,[29,63] H. Asano,[35,57] E. T. Atomssa,[63] T. C. Awes,[53] B. Azmoun,[7] V. Babintsev,[25] A. Bagoly,[17] M. Bai,[6] X. Bai,[11] B. Bannier,[63] K. N. Barish,[8] S. Bathe,[5,58] V. Baublis,[56] C. Baumann,[7] S. Baumgart,[57] A. Bazilevsky,[7] M. Beaumier,[8] R. Belmont,[13,68] A. Berdnikov,[60] Y. Berdnikov,[60] D. Black,[8] D. S. Blau,[34,49] M. Boer,[39] J. S. Bok,[51] K. Boyle,[58] M. L. Brooks,[39] J. Bryslawskyj,[5,8] H. Buesching,[7] V. Bumazhnov,[25] S. Butsyk,[50] S. Campbell,[14,29] V. Canoa Roman,[63] C.-H. Chen,[58] C. Y. Chi,[14] M. Chiu,[7] I. J. Choi,[26] J. B. Choi,[10,*] S. Choi,[61] P. Christiansen,[40] T. Chujo,[67] V. Cianciolo,[53] B. A. Cole,[14] M. Connors,[21,58] N. Cronin,[45,63] N. Crossette,[45] M. Csanád,[17] T. Csörgő,[18,70] T. W. Danley,[52] A. Datta,[50] M. S. Daugherity,[1] G. David,[7,63] K. DeBlasio,[50] K. Dehmelt,[63] A. Denisov,[25] A. Deshpande,[58,63] E. J. Desmond,[7] L. Ding,[29] J. H. Do,[71] L. D'Orazio,[42] O. Drapier,[36] A. Drees,[63] K. A. Drees,[6] J. M. Durham,[39] A. Durum,[25] T. Engelmore,[14] A. Enokizono,[57,59] S. Esumi,[67] K. O. Eyser,[7] B. Fadem,[45] W. Fan,[63] N. Feege,[63] D. E. Fields,[50] M. Finger,[9] M. Finger, Jr.,[9] F. Fleuret,[36] S. L. Fokin,[34] J. E. Frantz,[52] A. Franz,[7] A. D. Frawley,[20] Y. Fukao,[32] T. Fusayasu,[47] K. Gainey,[1] C. Gal,[63] P. Gallus,[15] P. Garg,[3,63] A. Garishvili,[65] I. Garishvili,[38] H. Ge,[63] F. Giordano,[26] A. Glenn,[38] X. Gong,[62] M. Gonin,[36] Y. Goto,[57,58] R. Granier de Cassagnac,[36] N. Grau,[2] S. V. Greene,[68] M. Grosse Perdekamp,[26] Y. Gu,[62] T. Gunji,[12] H. Guragain,[21] T. Hachiya,[48,58] J. S. Haggerty,[7] K. I. Hahn,[19] H. Hamagaki,[12] J. Hanks,[63] S. Hasegawa,[30] T. O. S. Haseler,[21] K. Hashimoto,[57,59] R. Hayano,[12] X. He,[21] T. K. Hemmick,[63] T. Hester,[8] J. C. Hill,[29] K. Hill,[13] A. Hodges,[21] R. S. Hollis,[8] K. Homma,[23] B. Hong,[33] T. Hoshino,[23] N. Hotvedt,[29] J. Huang,[7,39] S. Huang,[68] T. Ichihara,[57,58] Y. Ikeda,[57] K. Imai,[30] Y. Imazu,[57] M. Inaba,[67] A. Iordanova,[8] D. Isenhower,[1] A. Isinhue,[45] D. Ivanishchev,[56] B. V. Jacak,[63] S. J. Jeon,[46] M. Jezghani,[21] Z. Ji,[63] J. Jia,[7,62] X. Jiang,[39] B. M. Johnson,[7,21] K. S. Joo,[46] D. Jouan,[54] D. S. Jumper,[26] J. Kamin,[63] S. Kanda,[12,32] B. H. Kang,[22] J. H. Kang,[71] J. S. Kang,[22] J. Kapustinsky,[39] D. Kawall,[43] A. V. Kazantsev,[34] J. A. Key,[50] V. Khachatryan,[63] P. K. Khandai,[3] A. Khanzadeev,[56] K. M. Kijima,[23] C. Kim,[33] D. J. Kim,[31] E.-J. Kim,[10] M. Kim,[61] Y.-J. Kim,[26] Y. K. Kim,[22] D. Kincses,[17] E. Kistenev,[7] J. Klatsky,[20] D. Kleinjan,[8] P. Kline,[63] T. Koblesky,[13] M. Kofarago,[17,70] B. Komkov,[56] J. Koster,[58] D. Kotchetkov,[52] D. Kotov,[56,60] F. Krizek,[31] B. Kurgyis,[17] K. Kurita,[59] M. Kurosawa,[57,58] Y. Kwon,[71] R. Lacey,[62] Y. S. Lai,[14] J. G. Lajoie,[29] A. Lebedev,[29] D. M. Lee,[39] G. H. Lee,[10] J. Lee,[19,64] K. B. Lee,[39] K. S. Lee,[33] S. H. Lee,[29,63] M. J. Leitch,[39] M. Leitgab,[26] Y. H. Leung,[63] B. Lewis,[63] N. A. Lewis,[44] X. Li,[11] X. Li,[39] S. H. Lim,[39,71] M. X. Liu,[39] S. Lökös,[17,18] D. Lynch,[7] C. F. Maguire,[68] T. Majoros,[16] Y. I. Makdisi,[6] M. Makek,[69,72] A. Manion,[63] V. I. Manko,[34] E. Mannel,[7] M. McCumber,[13,39] P. L. McGaughey,[39] D. McGlinchey,[13,20,39] C. McKinney,[26] A. Meles,[51] M. Mendoza,[8] B. Meredith,[26] Y. Miake,[67] T. Mibe,[32] A. C. Mignerey,[42] D. E. Mihalik,[63] A. Milov,[69] D. K. Mishra,[4] J. T. Mitchell,[7] G. Mitsuka,[32,58] S. Miyasaka,[57,66] S. Mizuno,[57,67] A. K. Mohanty,[4] S. Mohapatra,[62] T. Moon,[71] D. P. Morrison,[7] S. I. Morrow,[68] M. Moskowitz,[45] T. V. Moukhanova,[34] T. Murakami,[35,57] J. Murata,[57,59] A. Mwai,[62] T. Nagae,[35] S. Nagamiya,[32,57] K. Nagashima,[23] J. L. Nagle,[13] M. I. Nagy,[17] I. Nakagawa,[57,58] Y. Nakamiya,[23] K. R. Nakamura,[35,57] T. Nakamura,[57] K. Nakano,[57,66] C. Nattrass,[65] P. K. Netrakanti,[4] M. Nihashi,[23,57] T. Niida,[67] R. Nouicer,[7,58] T. Novák,[18,70] N. Novitzky,[31,63] A. S. Nyanin,[34] E. O'Brien,[7] C. A. Ogilvie,[29] H. Oide,[12] K. Okada,[58] J. D. Orjuela Koop,[13] J. D. Osborn,[44] A. Oskarsson,[40] K. Ozawa,[32,67] R. Pak,[7] V. Pantuev,[27] V. Papavassiliou,[51] I. H. Park,[19,64] S. Park,[57,61,63] S. K. Park,[33] S. F. Pate,[51] L. Patel,[21] M. Patel,[29] J.-C. Peng,[26] W. Peng,[68] D. V. Perepelitsa,[13,14] G. D. N. Perera,[51] D. Yu. Peressounko,[34] C. E. PerezLara,[63] J. Perry,[29] R. Petti,[7,63] C. Pinkenburg,[7] R. P. Pisani,[7] M. L. Purschke,[7] H. Qu,[1] P. V. Radzevich,[60] J. Rak,[31] I. Ravinovich,[69] K. F. Read,[53,65] D. Reynolds,[62] V. Riabov,[49,56] Y. Riabov,[56,60] E. Richardson,[42] D. Richford,[5] T. Rinn,[29] N. Riveli,[52] D. Roach,[68] S. D. Rolnick,[8] M. Rosati,[29] Z. Rowan,[5] J. Runchey,[29] M. S. Ryu,[22] B. Sahlmueller,[63] N. Saito,[32] T. Sakaguchi,[7] H. Sako,[30] V. Samsonov,[49,56] M. Sarsour,[21] S. Sato,[30] S. Sawada,[32] B. K. Schmoll,[65] K. Sedgwick,[8] J. Seele,[58] R. Seidl,[57,58] Y. Sekiguchi,[12] A. Sen,[21,29] R. Seto,[8] P. Sett,[4] D. Sharma,[63] A. Shaver,[29] I. Shein,[25] T.-A. Shibata,[57,66] K. Shigaki,[23] M. Shimomura,[29,48] K. Shoji,[57] P. Shukla,[4] A. Sickles,[7,26] C. L. Silva,[39] D. Silvermyr,[40,53] B. K. Singh,[3] C. P. Singh,[3] V. Singh,[3] M. J. Skoby,[44] M. Skolnik,[45] M. Slunečka,[9] S. Solano,[45] R. A. Soltz,[38] W. E. Sondheim,[39] S. P. Sorensen,[65] I. V. Sourikova,[7] P. W. Stankus,[53] P. Steinberg,[7] E. Stenlund,[40] M. Stepanov,[43,*] A. Ster,[70] S. P. Stoll,[7] M. R. Stone,[13] T. Sugitate,[23] A. Sukhanov,[7] J. Sun,[63] Z. Sun,[16] A. Takahara,[12] A. Taketani,[57,58] Y. Tanaka,[47] K. Tanida,[30,58,61] M. J. Tannenbaum,[7] S. Tarafdar,[3,68] A. Taranenko,[49,62] E. Tennant,[51] R. Tieulent,[41] A. Timilsina,[29] T. Todoroki,[57,58,67] M. Tomášek,[15,28] H. Torii,[12] R. S. Towell,[1] I. Tserruya,[69] Y. Ueda,[23] B. Ujvari,[16] H. W. van Hecke,[39] M. Vargyas,[17,70] E. Vazquez-Zambrano,[14] A. Veicht,[14] J. Velkovska,[68] R. Vértesi,[70] M. Virius,[15] V. Vrba,[15,28] E. Vznuzdaev,[56] X. R. Wang,[51,58] D. Watanabe,[23] K. Watanabe,[57,59] Y. Watanabe,[57,58] Y. S. Watanabe,[12,32] F. Wei,[51] S. Whitaker,[29] S. Wolin,[26] C. P. Wong,[21] C. L. Woody,[7] M. Wysocki,[53] B. Xia,[52] C. Xu,[51] Q. Xu,[68] Y. L. Yamaguchi,[12,58,63] A. Yanovich,[25] S. Yokkaichi,[57,58] J. H. Yoo,[33] I. Yoon,[61] Z. You,[39] I. Younus,[37,50] H. Yu,[51,55] I. E. Yushmanov,[34] W. A. Zajc,[14] A. Zelenski,[6] S. Zharko,[60] S. Zhou,[11] and L. Zou[8]

(PHENIX Collaboration)

[1]*Abilene Christian University, Abilene, Texas 79699, USA*

[2]*Department of Physics, Augustana University, Sioux Falls, South Dakota 57197, USA*

[3]*Department of Physics, Banaras Hindu University, Varanasi 221005, India*

[4]*Bhabha Atomic Research Centre, Bombay 400 085, India*
[5]*Baruch College, City University of New York, New York, New York 10010, USA*
[6]*Collider-Accelerator Department, Brookhaven National Laboratory, Upton, New York 11973-5000, USA*
[7]*Physics Department, Brookhaven National Laboratory, Upton, New York 11973-5000, USA*
[8]*University of California-Riverside, Riverside, California 92521, USA*
[9]*Charles University, Ovocný trh 5, Praha 1, 116 36, Prague, Czech Republic*
[10]*Chonbuk National University, Jeonju, 561-756, Korea*
[11]*Science and Technology on Nuclear Data Laboratory, China Institute of Atomic Energy, Beijing 102413, People's Republic of China*
[12]*Center for Nuclear Study, Graduate School of Science, University of Tokyo, 7-3-1 Hongo, Bunkyo, Tokyo 113-0033, Japan*
[13]*University of Colorado, Boulder, Colorado 80309, USA*
[14]*Columbia University, New York, New York 10027 and Nevis Laboratories, Irvington, New York 10533, USA*
[15]*Czech Technical University, Zikova 4, 166 36 Prague 6, Czech Republic*
[16]*Debrecen University, H-4010 Debrecen, Egyetem tér 1, Hungary*
[17]*ELTE, Eötvös Loránd University, H-1117 Budapest, Pázmány P. s. 1/A, Hungary*
[18]*Eszterházy Károly University, Károly Róbert Campus, H-3200 Gyöngyös, Mátrai út 36, Hungary*
[19]*Ewha Womans University, Seoul 120-750, Korea*
[20]*Florida State University, Tallahassee, Florida 32306, USA*
[21]*Georgia State University, Atlanta, Georgia 30303, USA*
[22]*Hanyang University, Seoul 133-792, Korea*
[23]*Hiroshima University, Kagamiyama, Higashi-Hiroshima 739-8526, Japan*
[24]*Department of Physics and Astronomy, Howard University, Washington, DC 20059, USA*
[25]*IHEP Protvino, State Research Center of Russian Federation, Institute for High Energy Physics, Protvino 142281, Russia*
[26]*University of Illinois at Urbana-Champaign, Urbana, Illinois 61801, USA*
[27]*Institute for Nuclear Research of the Russian Academy of Sciences, prospekt 60-letiya Oktyabrya 7a, Moscow 117312, Russia*
[28]*Institute of Physics, Academy of Sciences of the Czech Republic, Na Slovance 2, 182 21 Prague 8, Czech Republic*
[29]*Iowa State University, Ames, Iowa 50011, USA*
[30]*Advanced Science Research Center, Japan Atomic Energy Agency, 2-4 Shirakata Shirane, Tokai-mura, Naka-gun, Ibaraki-ken 319-1195, Japan*
[31]*Helsinki Institute of Physics and University of Jyväskylä, P.O.Box 35, FI-40014 Jyväskylä, Finland*
[32]*KEK, High Energy Accelerator Research Organization, Tsukuba, Ibaraki 305-0801, Japan*
[33]*Korea University, Seoul 136-701, Korea*
[34]*National Research Center "Kurchatov Institute", Moscow 123098, Russia*
[35]*Kyoto University, Kyoto 606-8502, Japan*
[36]*Laboratoire Leprince-Ringuet, Ecole Polytechnique, CNRS-IN2P3, Route de Saclay, F-91128, Palaiseau, France*
[37]*Physics Department, Lahore University of Management Sciences, Lahore 54792, Pakistan*
[38]*Lawrence Livermore National Laboratory, Livermore, California 94550, USA*
[39]*Los Alamos National Laboratory, Los Alamos, New Mexico 87545, USA*
[40]*Department of Physics, Lund University, Box 118, SE-221 00 Lund, Sweden*
[41]*IPNL, CNRS/IN2P3, Univ Lyon, Université Lyon 1, F-69622, Villeurbanne, France*
[42]*University of Maryland, College Park, Maryland 20742, USA*
[43]*Department of Physics, University of Massachusetts, Amherst, Massachusetts 01003-9337, USA*
[44]*Department of Physics, University of Michigan, Ann Arbor, Michigan 48109-1040, USA*
[45]*Muhlenberg College, Allentown, Pennsylvania 18104-5586, USA*
[46]*Myongji University, Yongin, Kyonggido 449-728, Korea*
[47]*Nagasaki Institute of Applied Science, Nagasaki-shi, Nagasaki 851-0193, Japan*
[48]*Nara Women's University, Kita-uoya Nishi-machi Nara 630-8506, Japan*
[49]*National Research Nuclear University, MEPhI, Moscow Engineering Physics Institute, Moscow, 115409, Russia*
[50]*University of New Mexico, Albuquerque, New Mexico 87131, USA*
[51]*New Mexico State University, Las Cruces, New Mexico 88003, USA*
[52]*Department of Physics and Astronomy, Ohio University, Athens, Ohio 45701, USA*
[53]*Oak Ridge National Laboratory, Oak Ridge, Tennessee 37831, USA*
[54]*IPN-Orsay, Univ. Paris-Sud, CNRS/IN2P3, Université Paris-Saclay, BP1, F-91406, Orsay, France*
[55]*Peking University, Beijing 100871, People's Republic of China*
[56]*PNPI, Petersburg Nuclear Physics Institute, Gatchina, Leningrad region, 188300, Russia*
[57]*RIKEN Nishina Center for Accelerator-Based Science, Wako, Saitama 351-0198, Japan*
[58]*RIKEN BNL Research Center, Brookhaven National Laboratory, Upton, New York 11973-5000, USA*
[59]*Physics Department, Rikkyo University, 3-34-1 Nishi-Ikebukuro, Toshima, Tokyo 171-8501, Japan*
[60]*Saint Petersburg State Polytechnic University, St. Petersburg 195251, Russia*
[61]*Department of Physics and Astronomy, Seoul National University, Seoul 151-742, Korea*

[62]*Chemistry Department, Stony Brook University, SUNY, Stony Brook, New York 11794-3400, USA*
[63]*Department of Physics and Astronomy, Stony Brook University, SUNY, Stony Brook, New York 11794-3800, USA*
[64]*Sungkyunkwan University, Suwon 440-746, Korea*
[65]*University of Tennessee, Knoxville, Tennessee 37996, USA*
[66]*Department of Physics, Tokyo Institute of Technology, Oh-okayama, Meguro, Tokyo 152-8551, Japan*
[67]*Tomonaga Center for the History of the Universe, University of Tsukuba, Tsukuba, Ibaraki 305, Japan*
[68]*Vanderbilt University, Nashville, Tennessee 37235, USA*
[69]*Weizmann Institute, Rehovot 76100, Israel*
[70]*Institute for Particle and Nuclear Physics, Wigner Research Centre for Physics, Hungarian Academy of Sciences (Wigner RCP, RMKI) H-1525 Budapest 114, POBox 49, Budapest, Hungary*
[71]*Yonsei University, IPAP, Seoul 120-749, Korea*
[72]*Department of Physics, Faculty of Science, University of Zagreb, Bijenička c. 32 HR-10002 Zagreb, Croatia*

(Received 4 June 2018; published 19 November 2018)

Production of π^0 and η mesons has been measured at midrapidity in Cu+Au collisions at $\sqrt{s_{_{NN}}} = 200$ GeV. Measurements were performed in $\pi^0(\eta) \rightarrow \gamma\gamma$ decay channel in the 1(2)-20 GeV/c transverse momentum range. A strong suppression is observed for π^0 and η meson production at high transverse momentum in central Cu+Au collisions relative to the $p + p$ results scaled by the number of nucleon-nucleon collisions. In central collisions the suppression is similar to Au + Au with comparable nuclear overlap. The η/π^0 ratio measured as a function of transverse momentum is consistent with m_T-scaling parametrization down to $p_T = 2$ GeV/c, its asymptotic value is constant and consistent with Au + Au and $p + p$ and does not show any significant dependence on collision centrality. Similar results were obtained in hadron-hadron, hadron-nucleus, and nucleus-nucleus collisions as well as in e^+e^- collisions in a range of collision energies $\sqrt{s_{_{NN}}} = 3\text{–}1800$ GeV. This suggests that the quark-gluon-plasma medium produced in Cu+Cu collisions either does not affect the jet fragmentation into light mesons or it affects the π^0 and η the same way.

DOI: 10.1103/PhysRevC.98.054903

I. INTRODUCTION

Experiments at the Relativistic Heavy Ion Collider (RHIC) [1–4] and later at the Large Hadron Collider (LHC) [5–8] established the formation of quark-gluon plasma (QGP) in relativistic collisions of heavy ions (A+A). One of the most important tools to investigate the properties of this new medium are identified hadrons at high transverse momenta ($p_T > 5$ GeV/c), because they are leading fragments [9] of jets from hard-scattered partons, which, before fragmentation, interacted with the QGP [10]. The differential cross section of high-p_T hadron production in elementary $p + p$ collisions can be derived using next-to-leading-order perturbative-quantum-chromodynamics formalism [11,12]:

$$d\sigma_{pp\rightarrow hX} \approx \sum_{abcd} \int dx_a dx_b dz_c f_{a/p}(x_a) \otimes f_{b/p}(x_b) \otimes d\sigma_{ab\rightarrow cd} \otimes D_{c\rightarrow h}(z_c),$$

where $x_{a,b}$ is the initial momentum fraction carried by partons a and b, z_c is the final-state momentum fraction of the hadron h, $f_{a/p}$ and $f_{b/p}$ are the parton distribution functions (PDFs), $d\sigma_{ab\rightarrow cd}$ is the differential cross section of the initial partons hard scattering, $D_{c\rightarrow h}$ is the fragmentation function (FF) of the hard scattered parton to the final-state hadron.

There are two classes of nuclear effects, which modify the high-p_T hadron production cross section in A+A collisions. The initial state (or cold nuclear matter) effects are related to the presence of a heavy nucleus in the collision and require the modification of the corresponding PDF in Eq. (1). The correction factors for PDFs are usually obtained from the $p/d + A$ data [13,14].

The final-state effects are related to the formation of a hot, dense medium, QGP. While the hard-scattered parton propagates through the medium, it loses a fraction of its energy (jet-quenching) [10,15,16] by gluon emission or elastic scatterings with the medium constituents.

Parton energy loss in the QGP is quantified with the jet transport coefficient $\hat{q}$, defined as the squared momentum exchange between the hard parton and the medium per unit path length [10]. The relation of $\hat{q}$ to other medium parameters, such as temperature, shear viscosity, and entropy, is indicative of the character of the coupling to the medium [17].

Several phenomenological models [18–22] were designed to estimate $\hat{q}$ based on R_{AB} measurements at RHIC and the LHC. In the model calculations, the final-state effects are usually accounted for by replacing $D_{c\rightarrow h}$ with the medium-modified FF $\widetilde{D}_{c\rightarrow h}$ in Eq. (1). Methods of $\widetilde{D}_{c\rightarrow h}$ estimation are specific for each parton energy model. Also several attempts were made to extract $\hat{q}$ using lattice QCD calculations [23,24]. The effects of the medium on particle production

*Deceased.
†PHENIX Spokesperson: akiba@rcf.rhic.bnl.gov

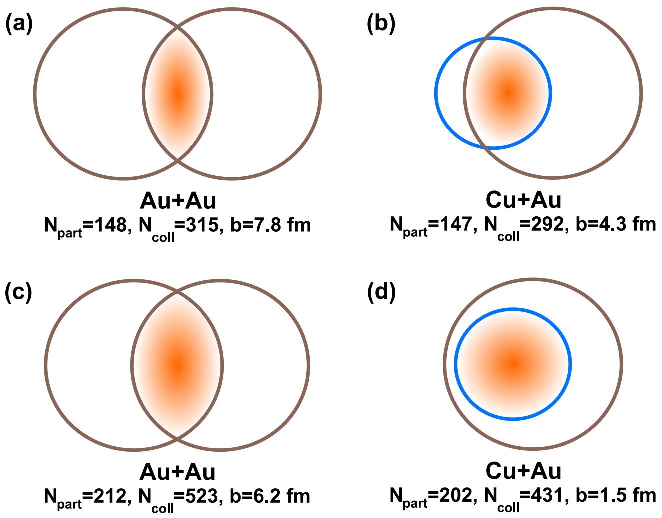

FIG. 1. Drawing showing Au+Au and Cu+Au collisions with comparable $N_{\rm part}$. On panel (b) the overlap area is asymmetric, and part of the dilute surfaces of Au and Cu (corona) overlap.

are usually quantified by the nuclear modification factor (R_{AB}):

$$R_{AB}^{\rm cent}(p_T) = \frac{1}{T_{AB}^{\rm cent}} \frac{dN_{AB}^{\rm cent}/dp_T}{d\sigma_{pp}/dp_T}, \quad (1)$$

where $dN_{AB}^{\rm cent}$ is the particle yield measured in A+B collisions for a given centrality class ($cent$), $d\sigma_{pp}$ is the cross section of the same particle measured in $p+p$ collisions at the same collision energy, $T_{AB}^{\rm cent}$ is the nuclear thickness function for the event class [25]. The energy loss of hard-scattered partons causes a reduction of R_{AB} from unity towards smaller values.

Measurement of π^0 meson production is particularly interesting, because π^0s are abundantly produced and their yields can be measured up to high p_T with good particle identification, an excellent signal-to-background ratio (S/B), and relatively small uncertainties using the electromagnetic calorimeters (EMCal) of the PHENIX detector. The η meson has four times heavier mass than π^0 and an about 50% strangeness content. Thus measurements of η allow us to study the dependence of jet quenching on the hadron mass and flavor content. Measurement of η/π^0 in A+A gives an opportunity to better understand whether fragmentation processes are affected by the presence of the colored medium.

Previously published results on π^0 and η production at PHENIX were obtained in symmetric heavy-ion systems such as Au+Au and Cu+Cu [26–30]. Contrarily to that, Cu+Au collisions at $\sqrt{s_{_{NN}}} = 200$ GeV is the first asymmetric system of heavy nuclei studied at RHIC. Such collisions provide a different collision geometry from the one realized in symmetric systems. In central collisions the Cu nucleus is fully submerged in the Au nucleus, which results in the reduction of nucleon-nucleon interactions in the corona region [31] of the collision (see Fig. 1). In semicentral Cu+Au collisions an asymmetry of the nuclear overlap region is present along the axis connecting the centers of the interacting nuclei. These features make Cu+Au collision system an important part of the systematic study of the final-state effects in heavy-ion collisions.

In this paper we present π^0 and η meson p_T spectra and nuclear modification factor measurements in Cu+Au collisions at $\sqrt{s_{_{NN}}} = 200$ GeV. Data were collected in RHIC Year-2012 run with the PHENIX detector.

II. DATA ANALYSIS

A detailed description of the PHENIX experimental setup can be found elsewhere [32]. Beam-beam counters (BBCs, $3.0 < |\eta| < 3.9$) [33] located downstream in both beam directions (north and south), each consisting of 64 Čerenkov-radiator counters, provide the minimum-bias (MB) trigger [34] and are also used to determine the event centrality and vertex position along the beam axis ($z_{\rm BBC}$). The MB trigger is formed if two or more BBC counters on each side detect the passage of charged particle(s). The MB trigger efficiency in Cu+Au is 93% of total inelastic collisions. The event centrality is defined by the total charge observed in the BBC. The mean number of participating nucleons ($N_{\rm part}$), binary collisions ($N_{\rm coll}$), and the nuclear overlap function (T_{AB}) in various centrality intervals are estimated with a Glauber-model Monte Carlo simulation [25] folded with the BBC response. The average values of T_{AB} and $N_{\rm part}$ for different centrality classes of Cu+Au collisions are listed in Table I.

The measurements are based on two data sets. Up to moderate p_T (< 8 GeV/c) 6.9×10^9 MB events satisfying a vertex cut of $|z_{\rm BBC}| < 20$ cm are used. To improve statistics and extend the range to higher p_T an additional sample was collected with one of the EMCal hardware triggers (ERT-A). This trigger required the presence of at least one high-energy shower in the EMCal. After off-line calibration it was found that the ERT-A trigger reached full efficiency for photons with energy above 4.5–5 GeV depending on location in the calorimeter. The accumulated ERT-A data sample after the same $|z_{\rm BBC}| < 20$ cm vertex cut corresponds to 1.8×10^{10} sampled MB events, which is a factor of three more than the MB sample. MB data is used to measure meson yields at $p_T <$ 8 GeV/c, and ERT-A data set is used at higher momenta.

Reconstruction of π^0 and η mesons is performed via their decay modes $\pi^0 \to \gamma\gamma$ and $\eta \to \gamma\gamma$. Photons are measured in the EMCal [35] located in the two central arms of the PHENIX detector, each covering 90° in azimuth and $|\eta| < 0.35$ in pseudorapidity. The EMCal comprises two

TABLE I. The average values of the nuclear thickness function $\langle T_{AB}\rangle$ and the numbers of nucleons participating in the nuclei interaction $\langle N_{\rm part}\rangle$ in different Cu+Au centrality intervals.

Centrality interval	$\langle T_{AB}\rangle$ (mb^{-1})	$\langle N_{\rm part}\rangle$
Minimum Bias	2.54 ± 0.19	61.1 ± 2.7
0%–10%	8.8 ± 0.6	177.2 ± 5.2
10%–20%	6.0 ± 0.4	132.4 ± 3.7
0%–20%	7.5 ± 0.5	154.8 ± 4.1
20%–40%	3.1 ± 0.2	80.4 ± 3.3
40%–60%	1.00 ± 0.12	34.9 ± 2.8

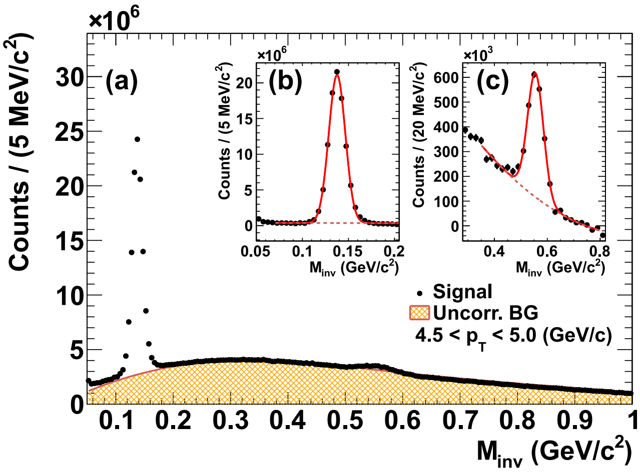

FIG. 2. Example of an invariant mass plot ($4.5 < p_T < 5.0$ GeV/c). (a) The foreground (photon pairs from the same event) is shown as points, the shaded area is the scaled mixed event background. Insert (b) shows the π^0 peak area after mixed event subtraction; the Gaussian fit to the peak and the first-order polynomial fit to the residual background are also shown. Insert (c) shows the η peak area with the Gaussian fit and second-order polynomial for the residual background.

technologically different subsystems: lead-scintillator sampling calorimeter (PbSc) and lead-glass Čerenkov calorimeter (PbGl), which cover 3/8 and 1/8 of the full azimuth, respectively. The PbSc and PbGl subsystems have different linearity, energy resolution ($\delta E/E = 2.1\% \oplus 8.1\%/\sqrt{E}$ for PbSc and $0.8\% \oplus 5.9\%/\sqrt{E}$ for PbGl) and segmentation ($\delta\phi \times \delta\eta \approx 0.01 \times 0.01$ for PbSc and 0.008×0.008 for PbGl).

The raw yields of π^0 and η mesons are determined from the $\gamma\gamma$ invariant mass ($m_{\rm inv}$) distribution, in bins of p_T and centrality. The analysis is carried out independently for the PbSc and PbGl subsystems. Photon candidates have to satisfy a shower shape cut [35] and are required to have energy (E_γ) larger than 0.4 GeV, which helps to further reduce the contribution from other particles, mostly minimum ionizing hadrons. Each $\gamma\gamma$ pair is required to satisfy an asymmetry cut $|\alpha| < 0.8$, where $\alpha = |E_{\gamma 1} - E_{\gamma 2}|/(E_{\gamma 1} + E_{\gamma 2})$. The asymmetry cut helps to reduce the background from combinatorial $\gamma\gamma$ pairs in the $m_{\rm inv}$ distributions, improving the S/B ratio. A typical invariant mass distribution is shown in Fig. 2.

The $m_{\rm inv}$ distributions contain two peaks in the selected mass region, which correspond to decays of π^0 and η. At lower p_T the peaks sit on top of a large combinatorial background. The shape of the background is estimated by event mixing, i.e., from the $m_{\rm inv}$ distribution obtained by combining photons from different events that nevertheless have similar collision vertex and centrality. The mixed event distributions are normalized and subtracted from the real event distributions. The mixed events are normalized outside of the meson peaks from $0.080 < m_{\rm inv} < 0.085$ and $0.3 < m_{\rm inv} < 0.4$ GeV/c^2 for the π^0 and $0.7 < m_{\rm inv} < 0.8$ GeV/c for the η. The combinatorial background decreases rapidly with increasing p_T, therefore, mixed event subtraction is carried out only for p_T below 7–10 GeV/c depending on the collision centrality. Above that the background under the peaks is estimated from the average counts in real events outside, but close to the peaks (sideband).

The resulting, combinatorial-subtracted invariant mass distributions are fit to a combination of a Gaussian to describe signal and a polynomial to describe the residual background. First- and second-order polynomials were used in π^0 and η measurements, respectively. Meson raw yields were obtained as the difference between the integral of the bin content in the mass peak regions and the integral of the polynomial fits to the residual background in the same region. The mass peak regions were defined as $m_{\rm inv} = 0.10$–0.17 and 0.48–0.62 GeV/c^2 for π^0 and η, respectively.

Acceptance and reconstruction efficiency (efficiency hereafter) are estimated using a GEANT3-based [36] Monte Carlo simulation of the PHENIX detector. The simulation was tuned to reproduce the observed mass peaks and widths of π^0 and η in the real data. To account for the effect of underlying events the simulated mesons were embedded in real data in each centrality, then analyzed with the same methods as the real data. Final efficiencies also account for branching ratios of the analyzed decay modes and for the ERT-A trigger efficiency in the corresponding data sample.

Invariant yields of π^0 and η are obtained as follows:

$$\frac{1}{N_{\rm event}} \frac{d^2N}{2\pi p_T dp_T dy} = \frac{N_{\rm raw}}{2\pi p_T N_{\rm event} \epsilon_{\rm rec} \Delta p_T \Delta y}, \qquad (2)$$

where $N_{\rm raw}$ is the particle raw yield and $\epsilon_{\rm rec}$ is the efficiency (including acceptance and all other corrections), $N_{\rm event}$ is the number of analyzed events.

Systematic uncertainties are classified into three types. Type A represents uncertainties, that are entirely p_T uncorrelated; these are added in quadrature to the statistical uncertainty. Type B uncertainties are p_T correlated, but different from point to point, and all data points can move up or down by the same fraction of their type-B uncertainty. Type C represents uncertainties, which move all points up or down by the same fraction. Typical values of the estimated systematic and total uncertainties are presented in Tables II and III.

One of the main sources of systematic uncertainties is the absolute energy calibration of the EMCal. The uncertainty on the absolute scale was estimated to be 1%. Due to the steeply falling (power-law) spectrum it corresponds to ≈2–9% uncertainty for the measured yields of π^0 and η mesons, which gradually increases from low to high momentum. At high p_T the measured π^0 yields are strongly affected by cluster merging when two photons from a π^0 decay have a small opening angle and produce partially or fully overlapping showers, which cannot be reconstructed as two individual clusters in the EMCal. Cluster merging results in significant loss of π^0 reconstruction efficiency at high p_T. Due to the different segmentation and Moliere radius [35] the merging effect manifests itself differently in the PbSc and PbGl subsystems. In PbSc the merging starts at $p_T > 12$ GeV/c, while in PbGl it starts only at $p_T > 16$ GeV/c. Uncertainties on how well the simulations describe the merging effect result in corresponding uncertainties for the measured π^0 yields, increase with p_T, reaching ≈20% in PbSc and ≈9% in PbGl

TABLE II. Systematic uncertainties for π^0 and η yields at different p_T. Values are shown for PbSc(PbGl) subsystems. The types of uncertainties are described in the text. Values with a range indicate the variation of the uncertainty over the different centrality intervals.

Source	$\pi^0 \rightarrow \gamma\gamma$		$\eta \rightarrow \gamma\gamma$		Type
	3.25 GeV/c	11 GeV/c	3.25 GeV/c	11 GeV/c	
Acceptance	1.5%(1.5%)	1.5%(1.5%)	1.5%(1.5%)	1.5%(1.5%)	B
p_T weights	1%(1%)	1%(1%)	1%(1%)	1%(1%)	B
Energy scale	5%(5%)	9%(9%)	5%(5%)	9%(9%)	B
Energy resolution	2%(2%)	2%(2%)	2%(2%)	2%(2%)	B
ERT-A efficiency	–	1%(1%)	–	1.3%(1.3%)	B
Photon conversion	5.2%(5.2%)	5.2%(5.2%)	5.2%(5.2%)	5.2%(5.2%)	C
Cluster merging	–	3%(2.5%)	–	–	B
PID cuts	4%(4%)–6%(4%)	4%(4%)–6%(4%)	5%(5%)–7%(5%)	5%(5%) – 7%(5%)	B
Raw yield extraction	3%(3%)	3%(3%)–4%(4%)	8.13%(8.13%)	5.3%(5.3%)	
Reconstruction efficiency	0.8%(1.5%)–1.7%(3%)	0.4%(0.7%)–0.7%(1.5%)	3%(5%)–4%(8%)	0.6%(1.2%) – 1.03%(1.9%)	A

at 20 GeV/c. Due to the four times heavier mass and larger $\gamma\gamma$ opening angle, the η measurements will be influenced by cluster merging only at $p_T > 50$ GeV/c, which is far beyond the p_T range presented in this analysis. At low p_T (below $\approx$5 GeV/c) the main uncertainty for π^0 and η comes from the raw yield extraction due to relatively small S/B ratios. This uncertainty is estimated as the maximum difference between raw yields obtained using different mass regions for mixed event background normalization, different fitting ranges, and different order polynomials for the residual background estimation. Some photons from π^0 and η decays convert into e^-e^+ pairs when traversing through detector material. If this happens within the magnetic field, they are bent in opposite directions and can not be reconstructed as a single photonlike cluster in the EMCal. As a result, $\approx$25% of π^0 and η mesons are lost. This effect is included in the efficiency calculation. The uncertainty on how accurately it is reproduced in the simulation is estimated to be 5.2%, and it is type C, because in the relevant energy range the conversion probability is almost constant.

Systematic uncertainties for η/π^0 ratios are included as a quadratic sum of the type-B uncertainties from π^0 and η yields. Because type-C uncertainties of the π^0 and η yields are 100% correlated between these particle measurements for all p_T, this uncertainty cancels in the ratios. The p_T-correlated systematic uncertainties for R_{AB} include both uncertainties from Cu+Au and $p + p$ measurements [12].

Invariant yields are obtained separately for PbSc and PbGl subsystems. The results are then averaged with weights defined by the quadratic sum of statistical and those systematic uncertainties that are uncorrelated between the two subsystems. The ratios of the yields obtained in PbSc and PbGl to the averaged ones are presented in Figs. 3(b)–3(d) and 3(f)–3(h). Only uncorrelated systematic uncertainties are shown in the ratios. Yields obtained in the different subsystems are consistent within statistical and uncorrelated systematic uncertainties. Typical systematic uncertainties for the combined spectra, π^0 and η R_{AB} and η/π^0 ratio are listed in Table III.

To facilitate comparison between different experiments and data sets, the data points of the meson spectra are plotted at

TABLE III. Total uncertainties for π^0 and η combined spectra, R_{AB} and η/π^0 ratios at different p_T. The types of uncertainties are described in the text. Values with a range indicate the variation of the uncertainty over different centrality intervals.

Type	3.25 GeV/c	11 GeV/c	3.25 GeV/c	11 GeV/c
	π^0 Combined Spectra		η Combined Spectra	
Stat	0.08%–0.2%	0.9%–4%	3%–5%	4%–11%
Type A	0.9%–1.8%	0.4%–0.9%	2%–4%	0.6%–0.9%
Type B	6%–7%	10.1%–10.3%	8.7%–9.3%	10.7%–11.1%
Type C	5.2%	5.2%	5.2%	5.2%
	π^0 R_{AB}		η R_{AB}	
Type A + Stat.	1.0%–1.9%	2.6%–4.4%	4%–6%	6%–13%
Type B	10.5%–10.7%	14.3%–14.4%	13.7%–14.1%	14.4%–14.7%
Type C	12%–23%	12%–23%	12%–23%	12%–23%
	η/π^0			
Type A + Stat.	4%–6%	4%–12%		
Type B	10.9%–11.4%	14.7%–15.1%		
Type C	–	–		

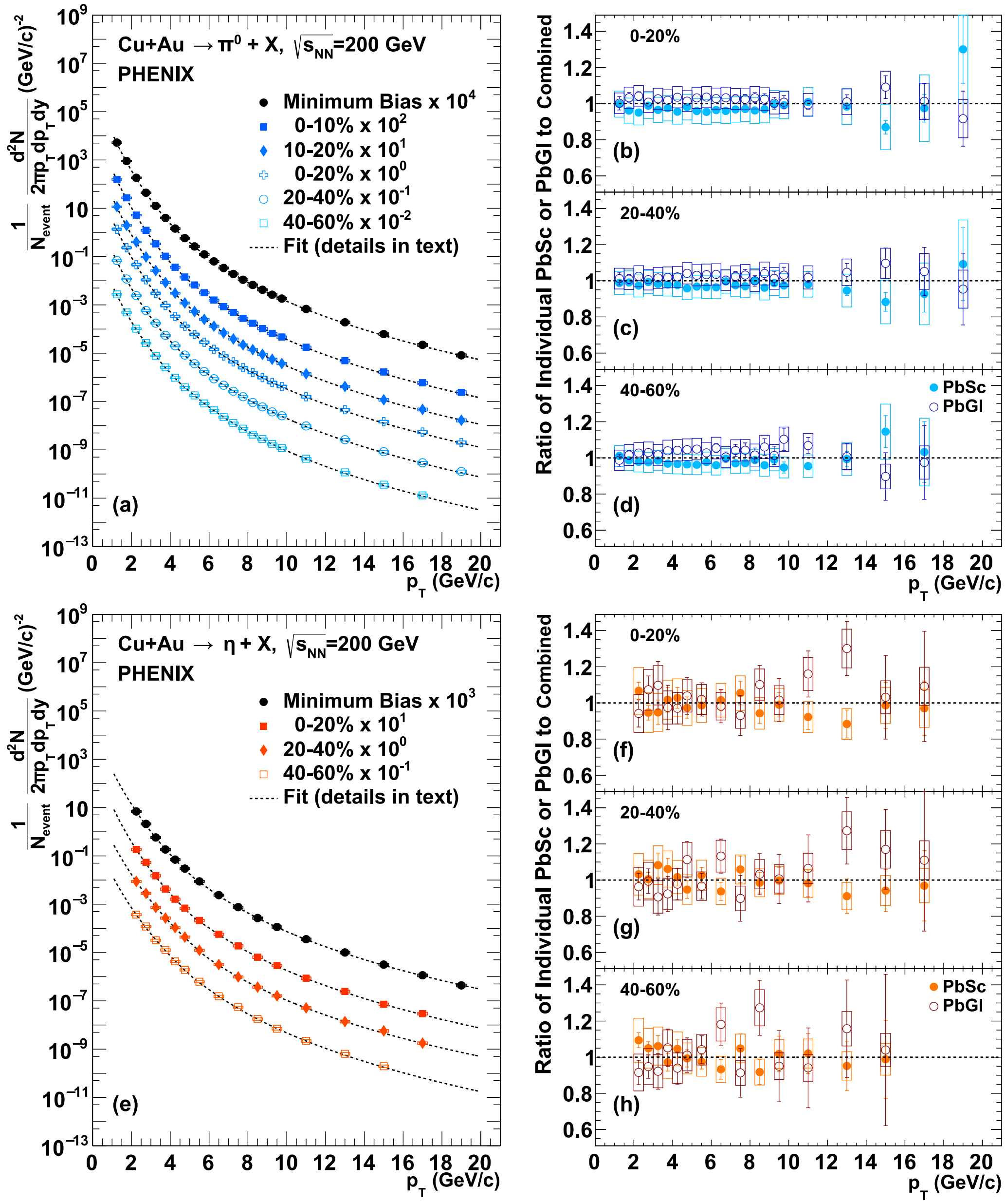

FIG. 3. Left: (a) π^0 and (b) η invariant p_T spectra measured in different centrality intervals of Cu+Au collisions at $\sqrt{s_{NN}} = 200$ GeV. The dashed curves are a fit with two Hagedorn-type functions with an asymptotic power-law (${p_T}^{-n}$) behavior. Right: ratios of (b)–(d) π^0 and (f)–(h) η yields measured in PbSc or PbGl subsystem to the averaged ones. Error bars represent a quadratic sum of statistical and type-A systematic uncertainties. Error boxes in the right panel correspond to the quadratic sum of systematic uncertainties, which are uncorrelated between PbSc and PbGl.

the center of each given p_T interval, which, due to the falling spectrum, does not represent the true physical value of the yield at that p_T [37]. A bin-shift correction is applied that adjusts the meson yields to their value at the bin center.

III. RESULTS AND DISCUSSION

Invariant yields in the p_T range 1(2)–20 GeV/c for π^0 (η) mesons measured in different centrality intervals and MB collisions are shown in Figs. 3(a) and 3(e), respectively. At low p_T the measurement is limited by the rapidly decreasing S/B ratio, and at high p_T by the available statistics.

Spectra of π^0 and η mesons can be fitted with a sum of Hagedorn and power-law functions:

$$f(p_T) = T(p_T)\frac{A}{(1+p_T/p_0)^m} + [1-T(p_T)]\frac{B}{p_T^n}, \qquad (3)$$

where $T(p_T) = 1/(1+\exp[(p_T - t)/w)]$, A, p_0, m, B, n, t, and w are free parameters. The parameter t governs at what p_T the second, pure power-law term becomes dominant; t varies between 4–6 GeV/c, depending on centrality. The parameter w varies between 0.05–0.15 GeV/c and governs the width of transition interval, where the first term loses its

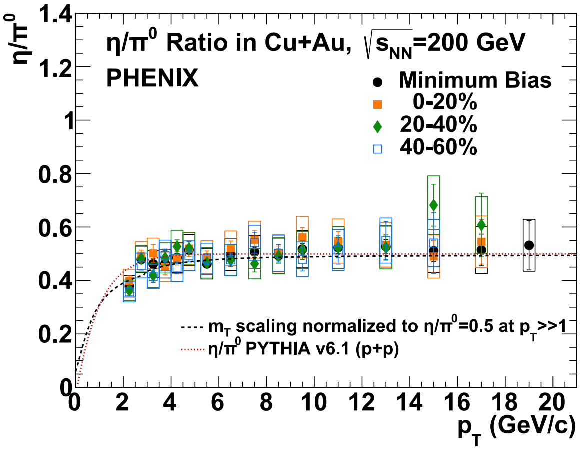

FIG. 4. Ratios of η and π^0 yields measured as a function of p_T in different centrality intervals of Cu+Au collisions at $\sqrt{s_{NN}} = 200$ GeV. Dashed curve shows the m_T scaling curve normalized to 0.5 at high momentum (see text). Error bars represent a quadratic sum of statistical and type-A systematic uncertainties for π^0 and η yields. Error boxes represent a quadratic sum of type-B systematic uncertainties for π^0 and η yields.

dominance and the second term becomes dominant. At high transverse momenta $f(p_T) \propto p_T{}^{-n}$. For π^0 in MB collisions $n = 8.06 \pm 0.01_{\text{stat}} \pm 0.06_{\text{sys}}$, for the most central 0%–10% collisions $n = 8.02 \pm 0.02_{\text{stat}} \pm 0.07_{\text{sys}}$, and increases slowly to $n = 8.07 \pm 0.02_{\text{stat}} \pm 0.06_{\text{sys}}$ up to 40% centrality. These numbers are consistent within uncertainties to the values obtained in pure power-law fits at high p_T (> 8 GeV/c) in 200 GeV Au+Au collisions with similar N_{part} [28,39].

The η/π^0 ratios (R_{η/π^0}) as a function of p_T for different Cu+Au centrality intervals are presented in the Fig. 4. Within uncertainties the measured R_{η/π^0} are centrality independent in the whole p_T range of measurements. A constant fit to the MB data in the $4 < p_T < 20$ GeV/c region results in $\eta/\pi^0 = 0.50 \pm 0.01_{\text{stat}} \pm 0.02_{\text{sys}}$, and the various centrality bins are consistent with this value. The dashed curve in Fig. 4 shows this asymptotically constant fit modified according to m_T scaling. Similar results were obtained in hadron-hadron, hadron-nucleus, and nucleus-nucleus collisions as well as in e^+e^- collisions in a wide range of collision energies $\sqrt{s_{NN}} = 3-1800$ GeV [26,40]. This suggests that QGP medium produced in Cu+Au collisions either does not affect the jet

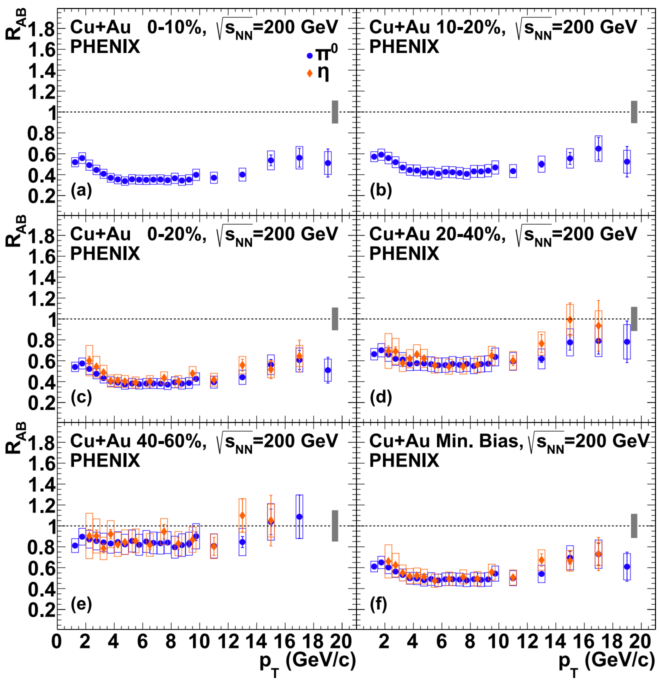

FIG. 5. R_{AB} of π^0 and η mesons measured as a function of p_T in different centrality intervals of Cu+Au collisions at $\sqrt{s_{NN}} = 200$ GeV. Error bars represent a quadratic sum of statistical and type-A systematic uncertainties from Cu+Au and $p+p$ measurements, respectively. Error boxes represent type-B systematic uncertainties from Cu+Au and $p+p$ measurements. Solid and open boxes at unity represent type-C systematic uncertainties from Cu+Au (including uncertainties from the T_{AB} values) and $p+p$, respectively. The reference $p+p$ measurements are published in Ref. [12] for π^0 and in Refs. [30,38] for η (see details in the text).

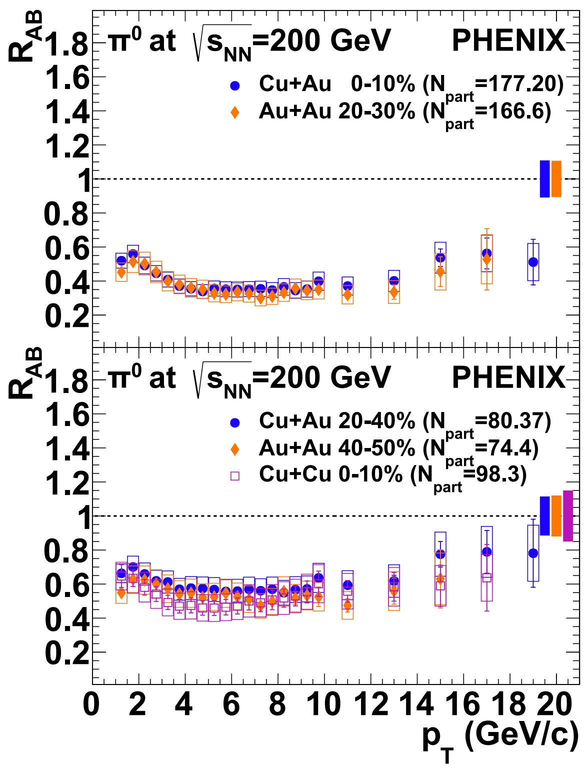

FIG. 6. Comparison of π^0 R_{AB} measured in Cu+Au, Au+Au and Cu+Cu collisions at $\sqrt{s_{NN}} = 200$ GeV and comparable N_{part}. Error bars represent a quadratic sum of statistical and type-A systematic uncertainties from Cu+Au and $p+p$ measurements. Open boxes are type-B systematic uncertainties for Cu+Au and $p+p$ collisions. The three boxes at unity are type-C systematic uncertainties from $p+p$ and heavy-ion collisions. The boxes from left to right correspond to Cu+Au, Au+Au and Cu+Cu measurements, respectively.

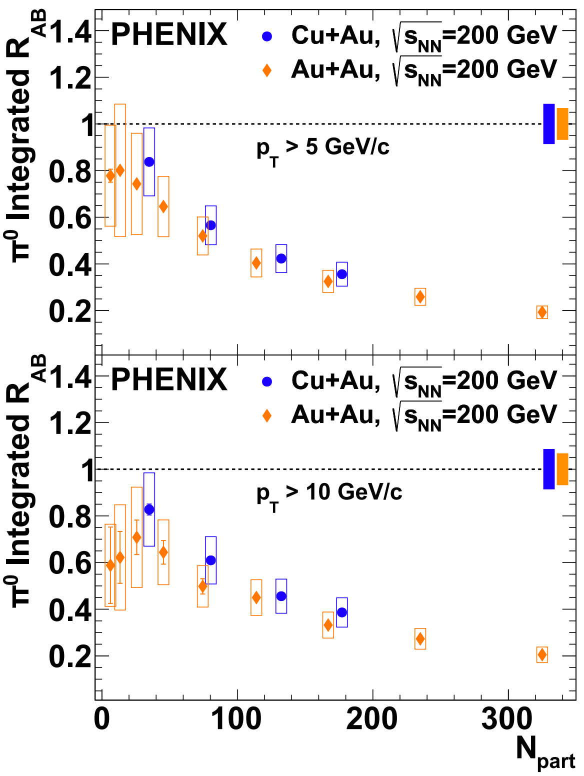

FIG. 7. Comparison of integrated R_{AB} for π^0 measured as a function of N_{part} in Cu+Au and Au+Au collisions at $\sqrt{s_{NN}} = 200$ GeV. Uncertainties are the same as in the Fig. 6. The lower limit of integration is $p_T = 5$ GeV/c on (a), $p_T = 10$ GeV/c on (b).

fragmentation into light mesons or it affects the π^0 and η the same way.

Nuclear modification factors of π^0 and η mesons as functions of p_T are shown in Fig. 5 for different Cu+Au centrality intervals. The reference π^0 meson production cross section in $p + p$ collisions was obtained from the 2005 PHENIX $p + p$ measurement [12]. For η meson R_{AB} estimation, the 2006 PHENIX $p + p$ measurements were used [38]. The R_{AB}'s of π^0 and η mesons are consistent within uncertainties in the whole p_T range for every analyzed centrality interval of Cu+Au collisions. At $p_T > 5$ GeV/c R_{AB} is ≈0.4–0.5 in most central collisions. A weak p_T dependence of the measured R_{AB} values can be observed. The suppression of π^0 and η decreases as one moves to more peripheral collisions.

Figure 6 compares R_{AB} of π^0 mesons measured as a function of p_T in Cu+Au, Au+Au [28], and Cu+Cu [29] collisions at $\sqrt{s_{NN}} = 200$ GeV and similar N_{part}. In central and semicentral Cu+Au collisions π^0 R_{AB} are consistent with those measured in Au+Au and Cu+Cu, if applicable, which suggests that π^0 suppression mostly depends on the energy density and size of the produced medium. Because in the most central collisions the Cu ion is fully submerged in Au, without any corona [31], but the suppression is the same as in Au+Au at comparable N_{part}, the corona effect is either nonexistent or very small.

In Fig. 7, the π^0 and η integrated R_{AB}'s are shown as a function of N_{part} and compared to Au+Au. The integration is carried out in two different p_T ranges ($p_T > 5$ GeV/c and $p_T > 10$ GeV/c). The results obtained for the two different collision systems are consistent within uncertainties.

IV. SUMMARY

In summary, PHENIX has measured π^0 and η invariant p_T spectra and nuclear modification factors in asymmetric collisions of heavy ions, Cu+Au at $\sqrt{s_{NN}} = 200$ GeV in a wide p_T range $[1(2) < p_T < 20$ GeV/$c]$ and for several centrality intervals. In the more central collisions the spectra are similar to those observed in Au+Au. The asymptotic (high p_T) value of η/π^0 is $0.50 \pm 0.01_{\text{stat}} \pm 0.02_{\text{sys}}$, constant, independent of collision centrality, and consistent with the previously measured values in hadron-hadron, hadron-nucleus, nucleus-nucleus, as well as e^+e^- collisions at $\sqrt{s_{NN}} = 3$–1800 GeV, suggesting that either the fragmentation of jets into π^0 and η is unchanged irrespective of the absence or presence of the medium, or it changes the same way, despite the different flavor content. The values of R_{AB} for π^0 and η are consistent within uncertainties in all analyzed centrality intervals of Cu+Au collisions. The suppression pattern of π^0 in Cu+Au collisions is consistent with Au+Au and Cu+Cu collisions at the same interaction energy and similar values of N_{part}.

ACKNOWLEDGMENTS

We thank the staff of the Collider-Accelerator and Physics Departments at Brookhaven National Laboratory and the staff of the other PHENIX participating institutions for their vital contributions. We acknowledge support from the Office of Nuclear Physics in the Office of Science of the Department of Energy, the National Science Foundation, Abilene Christian University Research Council, Research Foundation of SUNY, and Dean of the College of Arts and Sciences, Vanderbilt University (U.S.A), Ministry of Education, Culture, Sports, Science, and Technology and the Japan Society for the Promotion of Science (Japan), Conselho Nacional de Desenvolvimento Científico e Tecnológico and Fundação de Amparo à Pesquisa do Estado de São Paulo (Brazil), Natural Science Foundation of China (People's Republic of China), Croatian Science Foundation and Ministry of Science and Education (Croatia), Ministry of Education, Youth and Sports (Czech Republic), Centre National de la Recherche Scientifique, Commissariat à l'Énergie Atomique, and Institut National de Physique Nucléaire et de Physique des Particules (France), Bundesministerium für Bildung und Forschung, Deutscher Akademischer Austausch Dienst, and Alexander von Humboldt Stiftung (Germany), J. Bolyai Research Scholarship, EFOP, the New National Excellence Program (ÚNKP), NKFIH, and OTKA (Hungary), Department of Atomic Energy and Department of Science and Technology (India), Israel Science Foundation (Israel), Basic Science Research Program through NRF of the Ministry of Education (Korea), Physics Department, Lahore University of Management Sciences (Pakistan), Ministry of Education and Science, Russian Academy of Sciences, Federal Agency of Atomic Energy (Russia), VR and Wallenberg Foundation (Sweden), the U.S. Civilian Research and

Development Foundation for the Independent States of the Former Soviet Union, the Hungarian American Enterprise Scholarship Fund, the US-Hungarian Fulbright Foundation, and the US-Israel Binational Science Foundation.

[1] I. Arsene *et al.* (BRAHMS Collaboration), Quark gluon plasma and color glass condensate at RHIC? The Perspective from the BRAHMS experiment, Nucl. Phys. A **757**, 1 (2005).
[2] B. B. Back *et al.*, The PHOBOS perspective on discoveries at RHIC, Nucl. Phys. A **757**, 28 (2005).
[3] J. Adams *et al.* (STAR Collaboration), Experimental and theoretical challenges in the search for the quark gluon plasma: The STAR Collaboration's critical assessment of the evidence from RHIC collisions, Nucl. Phys. A **757**, 102 (2005).
[4] K. Adcox *et al.* (PHENIX Collaboration), Formation of dense partonic matter in relativistic nucleus-nucleus collisions at RHIC: Experimental evaluation by the PHENIX collaboration, Nucl. Phys. A **757**, 184 (2005).
[5] S. Chatrchyan *et al.* (CMS Collaboration), Study of high-pT charged particle suppression in PbPb compared to *pp* collisions at $\sqrt{s_{NN}} = 2.76$ TeV, Eur. Phys. J. C **72**, 1945 (2012).
[6] B. Abelev *et al.* (ALICE Collaboration), Centrality dependence of charged particle production at large transverse momentum in Pb–Pb collisions at $\sqrt{s_{NN}} = 2.76$ TeV, Phys. Lett. B **720**, 52 (2013).
[7] G. Aad *et al.* (ATLAS Collaboration), Measurement of the jet radius and transverse momentum dependence of inclusive jet suppression in lead-lead collisions at $\sqrt{s_{NN}} = 2.76$ TeV with the ATLAS detector, Phys. Lett. B **719**, 220 (2013).
[8] T. Gunji (ALICE Collaboration), Overview of recent ALICE results, Nucl. Phys. A **956**, 11 (2016).
[9] M. Jacob and P. V Landshoff, Large transverse momentum and jet studies, Phys. Rep. **48**, 285 (1978).
[10] R. Baier, D. Schiff, and B. G. Zakharov, Energy loss in perturbative QCD, Ann. Rev. Nucl. Part. Sci. **50**, 37 (2000).
[11] J. F. Owens, Large momentum transfer production of direct photons, jets, and particles, Rev. Mod. Phys. **59**, 465 (1987).
[12] A. Adare *et al.* (PHENIX Collaboration), Inclusive cross-section and double helicity asymmetry for π^0 production in $p+p$ collisions at $\sqrt{s} = 200$ GeV: Implications for the polarized gluon distribution in the proton, Phys. Rev. D **76**, 051106 (2007).
[13] I. Helenius, K. J. Eskola, H. Honkanen, and C. A. Salgado, Impact-parameter dependent nuclear parton distribution functions: EPS09s and EKS98s and their applications in nuclear hard processes, J. High Energy Phys. 07 (2012) 073.
[14] K. J. Eskola, P. Paakkinen, H. Paukkunen, and C. A. Salgado, EPPS16: Nuclear parton distributions with LHC data, Eur. Phys. J. C **77**, 163 (2017).
[15] J. D. Bjorken, Energy Loss of Energetic Partons in Quark - Gluon Plasma: Possible Extinction of High p(t) Jets in Hadron - Hadron Collisions, (1982), FERMILAB-PUB-82-059-THY, FERMILAB-PUB-82-059-T.
[16] X.-N. Wang, M. Gyulassy, and M. Plumer, The LPM effect in QCD and radiative energy loss in a quark gluon plasma, Phys. Rev. D **51**, 3436 (1995).
[17] A. Majumder, B. Müller, and X.-N. Wang, Small Shear Viscosity of a Quark-Gluon Plasma Implies Strong Jet Quenching, Phys. Rev. Lett. **99**, 192301 (2007).
[18] G.-Y. Qin, J. Ruppert, C. Gale, S. Jeon, G. D. Moore, and M. G. Mustafa, Radiative and Collisional Jet Energy Loss in the Quark-Gluon Plasma at RHIC, Phys. Rev. Lett. **100**, 072301 (2008).
[19] X.-F. Chen, T. Hirano, E. Wang, X.-N. Wang, and H. Zhang, Suppression of high-p_T hadrons in Pb+Pb collisions at energies available at the CERN-Large Hadron Collider, Phys. Rev. C **84**, 034902 (2011).
[20] C. Young, B. Schenke, S. Jeon, and C. Gale, MARTINI event generator for heavy quarks: Initialization, parton evolution, and hadronization, Phys. Rev. C **86**, 034905 (2012).
[21] A Majumder and C Shen, Suppression of the High-p_T Charged-Hadron R_{AA} at the LHC, Phys. Rev. Lett. **109**, 202301 (2012).
[22] J. Xu, A. Buzatti, and M. Gyulassy, Azimuthal jet flavor tomography with CUJET2.0 of nuclear collisions at RHIC and LHC, J. High Energy Phys. 08 (2014) 063.
[23] A. Majumder, Calculating the jet quenching parameter $\hat{q}$ in lattice gauge theory, Phys. Rev. C **87**, 034905 (2013).
[24] M. Panero, K. Rummukainen, and A. Schäfer, Lattice Study of the Jet Quenching Parameter, Phys. Rev. Lett. **112**, 162001 (2014).
[25] M. L. Miller, K. Reygers, S. J. Sanders, and P. Steinberg, Glauber modeling in high energy nuclear collisions, Ann. Rev. Nucl. Part. Sci. **57**, 205 (2007).
[26] S. S. Adler *et al.* (PHENIX Collaboration), High transverse momentum η meson production in $p+p$, $d+$Au and Au$+$Au collisions at $\sqrt{s_{NN}} = 200$ GeV, Phys. Rev. C **75**, 024909 (2007).
[27] A. Adare *et al.* (PHENIX Collaboration), Quantitative constraints on the opacity of hot partonic matter from semi-inclusive single high transverse momentum pion suppression in Au+Au collisions at $\sqrt{s_{NN}} = 200$ GeV, Phys. Rev. C **77**, 064907 (2008).
[28] A. Adare *et al.* (PHENIX Collaboration), Suppression Pattern of Neutral Pions at High Transverse Momentum in Au+Au Collisions at $\sqrt{s_{NN}} = 200$-GeV and Constraints on Medium Transport Coefficients, Phys. Rev. Lett. **101**, 232301 (2008).
[29] A. Adare *et al.* (PHENIX Collaboration), Onset of π^0 Suppression Studied in Cu+Cu Collisions at $\sqrt{s_{NN}} = 22.4$, 62.4, and 200 GeV, Phys. Rev. Lett. **101**, 162301 (2008).
[30] A. Adare *et al.* (PHENIX Collaboration), Transverse momentum dependence of η meson suppression in Au+Au collisions at $\sqrt{s_{NN}} = 200$ GeV, Phys. Rev. C **82**, 011902 (2010).
[31] V. S. Pantuev, Jet absorption and corona effect at RHIC: Extracting collision geometry from experimental data, JETP Lett. **85**, 104 (2007).
[32] K. Adcox *et al.* (PHENIX Collaboration), PHENIX detector overview, Nucl. Instrum. Methods Phys. Res., Sec. A **499**, 469 (2003).
[33] M. Allen *et al.* (PHENIX Collaboration), PHENIX inner detectors, Nucl. Instrum. Methods Phys. Res., Sec. A **499**, 549 (2003).
[34] S. S. Adler *et al.* (PHENIX Collaboration), PHENIX on-line systems, Nucl. Instrum. Methods Phys. Res., Sec. A **499**, 560 (2003).

[35] L. Aphecetche *et al.* (PHENIX Collaboration), PHENIX calorimeter, Nucl. Instrum. Methods Phys. Res., Sec. A **499**, 521 (2003).

[36] R. Brun, R. Hagelberg, M. Hansroul, and J. C. Lassalle, GEANT: Simulation Program for Particle Physics Experiments. User Guide and Reference Manual, 1978, CERN-DD-78-2-REV.

[37] G. D. Lafferty and T. R. Wyatt, Where to stick your data points: The treatment of measurements within wide bins, Nucl. Instrum. Methods Phys. Res., Sec. A **355**, 541 (1995).

[38] A. Adare *et al.* (PHENIX Collaboration), Cross section and double helicity asymmetry for η mesons and their comparison to neutral pion production in $p+p$ collisions at $\sqrt{s} = 200$ GeV, Phys. Rev. D **83**, 032001 (2011).

[39] A. Adare *et al.* (PHENIX Collaboration), Neutral pion production with respect to centrality and reaction plane in Au+Au collisions at $\sqrt{s_{NN}} = 200$ GeV, Phys. Rev. C **87**, 034911 (2013).

[40] F. W. Busser *et al.*, A Study of high transverse momentum η and π^0 Mesons at the CERN ISR, Phys. Lett. B **55**, 232 (1975).